Applied Surface Science 531 (2020) 147394

Contents lists available at ScienceDirect

Applied Surface Science

journal homepage: www.elsevier.com/locate/apsusc

# Highly efficient visible light phenyl modified carbon nitride/$TiO_2$ photocatalyst for environmental applications

Stefania Porcu[a], Micaela Castellino[b], Ignazio Roppolo[b], Carlo Maria Carbonaro[a], Simonetta Palmas[c], Laura Mais[c], Maria Francesca Casula[c], Svetlana Neretina[d], Robert A. Hughes[d], Francesco Secci[e], Pier Carlo Ricci[a,*]

[a] Department. of Physics, University of Cagliari, S.p. no. 8 Km 0,700, 09042 Monserrato (Ca), Italy
[b] Department of Applied Science and Technology, Politecnico di Torino, Corso Duca degli Abruzzi 24, Torino 10129, Italy
[c] Department of Mechanical, Chemical, and Materials Engineering INSTM and University of Cagliari, Via Marengo, 3, 09123 Cagliari, Italy
[d] Department of Aerospace and Mechanical Engineering, University of Notre Dame, 370 Fitzpatrick Hall, Notre Dame, IN 46556, United States
[e] Department of Chemical and Geological Science, University of Cagliari, S.p. no. 8 Km0700, 09042 Monserrato (Ca), Italy

ARTICLE INFO

*Keywords:*
Photocatalyst
Carbon nitride
Organic-inorganic hybrid materials

ABSTRACT

Eco-sustainable solutions for the neutralization of air and water pollutants have increasingly gravitated toward the use of heterogeneous photocatalysts. This approach, which transforms pollutants into harmless substances through a light-driven chemical reaction on a catalytic surface, must comply with eco-sustainability requirements and be easily applicable. Semiconductor-based photocatalysis is a promising pathway for the degradation of environmental pollutants and, among all the various semiconductors used, titanium dioxide has proved itself to be the foremost material for environmental remediation due to its highly desirable photocatalytic properties. Titanium dioxide, however, poorly exploits the visible part of the electromagnetic spectrum due to the relatively large band-gap of its anatase phase, and as such, the UV portion of the solar spectrum is largely responsible for its photocatalytic activity. Herein, we demonstrate a highly efficient visible light hybrid catalyst based on titanium dioxide and phenyl carbon nitride (PhCN). With the organic component providing a broad absorption up to 600 nm and fast charge exchange to the conduction band of $TiO_2$, the combination allows for the highly efficient photocatalytic degradation of Rhodamine B under visible excitation.

## 1. Introduction

With applications in water splitting, solar energy conversion, and environmental remediation [1–3], semiconductor-based photocatalysts represent a potentially disruptive technology. The exploitation of solar radiation helps to meet the ever-increasing demand for energy and address the need to mitigate the impact of anthropogenic pollutants.

To better exploit solar energy will require the discovery of new photocatalysts with high efficiency in the visible range of the solar spectrum. The necessity arises from the fact that such photocatalysts can utilize the sizeable visible component of the solar spectrum (up to 43%) whereas those reliant on higher energy photons are inherently limited by the relatively low intensities in the ultraviolet (UV) ($\approx$ 5%) [4]. Consequently, several novel photocatalytic materials and systems have recently emerged as promising candidates. Currently, the most attractive photocatalytic materials are n-type semiconductors such as $TiO_2$, $WO_3$, and $Fe_2O_3$ because of their high chemical stability and a conduction band edge with a potential level that is negative enough to allow the proton reduction without additional electric bias [5–7]. None of these materials, however, demonstrate significant absorption in the visible part of the spectrum, thus substantially reduces their technological viability.

The strong oxidizing capability of $TiO_2$ [4,8–10] has made it one of the most widely studied and applied semiconductor photocatalysts. Nevertheless, its high band gap (3.2 eV) stands out as a major disadvantage because it leads to negligible light harvesting in the visible range [4]. Indeed, the photocatalytic properties of $TiO_2$ are reliant upon the excitation of photogenerated charge carriers above its band gap through the absorption of UV light. In an effort to increase the photoactivity of $TiO_2$ in the visible light range, various strategies have been forwarded such as ion doping [11,12] or the formation of $TiO_2$-based heterostructures with a lower band gap [13–15]. In particular, the organic-inorganic hybrid system that couples $TiO_2$ to graphitic carbon nitride (g-$C_3N_4$) represents an intriguing solution because it meshes the

* Corresponding author.
*E-mail address:* carlo.ricci@dsf.unica.it (P.C. Ricci).

https://doi.org/10.1016/j.apsusc.2020.147394
Received 23 April 2020; Received in revised form 23 July 2020; Accepted 27 July 2020
Available online 30 July 2020
0169-4332/ 

photocatalytic properties of $TiO_2$ with the lower band gap energy (2.7 eV) and thermal and chemical stability of g-$C_3N_4$ [16,17] Additionally, the delocalized conjugated structure of g-$C_3N_4$ gives rise to a slow charge recombination rate and a rapid photoinduced charge separation. Despite these positive attributes, the efficiency of g-$C_3N_4$ as a standalone photocatalytic material is diminished by a low quantum efficiency and high recombination rate of photogenerated electron–hole pairs [18,19]. In contrast, the formation of a charge-transfer complex at the interface between the organic donor (i.e., g-$C_3N_4$) and inorganic acceptor (i.e., $TiO_2$) compound results in a g-$C_3N_4$/$TiO_2$ heterojunction system that shows a decrease in the recombination rate of photogenerated electron–hole pairs as well as an increase in the photocatalytic activity of $TiO_2$ under visible light for wavelengths as low as 450 nm [21–23].

If hybrid systems have to show superior performance as photocatalysts, then the next challenge is to red shift the working spectral range so as to utilize a larger portion of the visible solar spectrum. From this perspective, phenyl-carbon nitride (PhCN) is a promising candidate material due to its lower band gap (2.0 eV) and a recombination rate photoexcited carriers that is slower than pure g-$C_3N_4$ [24]. Herein, we demonstrate the synthesis of the PhCN/$TiO_2$ heterojunction system and validate it as an efficient catalyst for the photodegradation of Rhodamine B (RhB) and methylene blue (MB) under visible light irradiation. It is shown that the heterojunction system can be obtained using a two-step synthetic method, in which titanium tetrachloride ($TiCl_4$), ascorbic acid, and phenyl-carbon nitride precursors are exposed to a hydrothermal treatment followed by calcination. Using time-resolved photoluminescence and X-ray photoelectron spectroscopy, the reaction product is shown to be a genuine hybrid structure that exhibits improved features connected to the mutual interaction of pure organic and inorganic segments that are chemically distinct and interacting.

The photocatalytic performance was tested in a model system, by the degradation of Rhodamine B and methylene blue under commercial white LED to prove the efficiency in the visible part of the spectrum. The photocatalytic performance of the PhCN/$TiO_2$ hybrid system for the decomposition of Rhodamine B (RhB) under visible light as compared to $TiO_2$ and to g-$C_3N_4$/$TiO_2$ hybrid system foster PhCN/$TiO_2$ hybrid as effective photocatalyst operating under visible light source.

## 2. Experimental section

### 2.1. Materials and methods

#### 2.1.1. Materials

Ph-Triazine (99%), melamine (99%), titanium (IV) chloride (99%), Rhodamine B (95%) Methylene blue and L-ascorbic acid (99%) were purchased from Sigma Aldrich. Absolute ethanol (94–96%) was sourced from Alfa Aesar. All chemicals were used as received without further purification. Deionized (DI) water was used in the preparation of the Rhodamine aqueous solution.

#### 2.1.2. Preparation of PhCN and g-$C_3N_4$

PhCN was prepared by placing 1 g of 6-phenyl-1,3,5-triazine-2,4-diamine powder (Ph-Triazine) in a quartz tube accommodated in a tubular furnace and heated to 400 °C for 1 h. Similarly, g-$C_3N_4$ was prepared by heating 1 g of melamine to 550 °C for 1 h.

For both thermal treatments, samples were covered with a quartz plate to prevent the vaporization and to insure re-condensation at high temperatures. The heating rate was 30 °C·min$^{-1}$ and the synthesis was performed under a constant flow of nitrogen gas (30 mL·min$^{-1}$). The heat-treated material was manually ground to obtain powder-like samples and several times washed with methanol to remove impurities [24].

#### 2.1.3. Preparation of PhCN/$TiO_2$, g-$C_3N_4$/$TiO_2$ heterojunction systems and pure a-$TiO_2$

Both the PhCN/$TiO_2$ and g-$C_3N_4$/$TiO_2$ heterojunction systems were prepared by a facile hydrothermal method followed by calcination. PhCN (0.02 g) and g-$C_3N_4$ (0.02 g) were each dispersed in 15 mL of ethyl alcohol and magnetically stirred for 30 min. Ascorbic acid (0.075 g) was then added to each suspension. $TiCl_4$ aqueous solution (0.5 mL) was then added while continuously undergoing magnetic stirring for 20 min. Each solution was then transferred to a 50 mL Teflon-lined autoclave that was oven heated to 180 °C for 8 h. Once cooled down to room temperature, the products were 4-times washed with DI water and absolute alcohol followed by a 12 h drying procedure at 60 °C. The powders were calcinated at 400 °C for 2 h to obtain white powders of PhCN- $TiO_2$ and g-$C_3N_4$-$TiO_2$ hybrid samples.

$TiO_2$ in anatase phase was synthesized using the hydrothermal procedure above described without the adding of the organic compounds.

### 2.2. Characterization techniques

A combination of analytical techniques was used allowing the full characterization of the PhCN–$TiO_2$ and g-$C_3N_4$-$TiO_2$ synthesized samples.

#### 2.2.1. Raman spectroscopy

Raman measurements were carried out on $TiO_2$ samples in the backscattering geometry using the 532 nm line sourced from a wavelength stabilized diode module (LASOS DPSS series) that is coupled to a Reflecting Bragg Grating (Optigrate-Braggrade 532) so as to narrow the laser linewidth. Measurements were performed at room temperature with a Raman spectrometer MS-750 Sol Instruments system with a spectral resolution of 1 cm$^{-1}$. Spectra were recorded in the Stokes region using a 1200 groove·mm$^{-1}$ grating monochromator. In order to avoid a luminescence background, the Raman spectra of pure PhCN, and of PhCN/$TiO_2$ hybrid system were collected using the 1064 nm excitation wavelength generated by a Nd:YAG laser. The measurements were performed in air at room temperature with a BWTEK iRaman spectrometer with a spectral resolution of 9 cm$^{-1}$.

#### 2.2.2. Absorption measurements

Absorption measurements were obtained by diffuse reflectance spectroscopy utilizing a UV–Vis-NIR Agilent Technologies Cary 5000 Spectrometer. Measurements were performed by using a PbS solid-state photodetector. The reflection configuration measures the diffuse reflection of the sample with respect to a KBr reference that is considered to have a 100% reflectivity. The Kubelka-Munck equation was applied to extract the absorption features.

#### 2.2.3. Photoluminescence (PL)

Steady-state photoluminescence measurements were performed with a 405 nm laser excitation wavelength that is coupled to an Avantes Sensilne Avaspec-ULS-TEC Spectrometer with an optical fiber. The measurements were acquired with a 500 ms time window in a 300–800 nm spectral range.

#### 2.2.4. Time-resolved photoluminescence (TR-PL) measurements

Time-resolved photoluminescence (TR-PL) measurements were recorded by exciting the samples with 200 fs pulses sourced from an optical parametric amplifier (Light Conversion TOPAS-C) pumped by a regenerative Ti:Sapphire amplifier (Coherent Libra-HE). The repetition frequency was 1 kHz and the TR-PL signal was recorded by a streak camera (Hamamatsu C10910) equipped with a grating spectrometer (Princeton Instruments Acton Spectra Pro SP-2300). All the measurements were collected in the front-face configuration to reduce inner filter effects. Proper emission filters were applied to remove the reflected contribution of the excitation light.

#### 2.2.5. Scanning electron microscopy (SEM)

SEM studies were carried out using a Carl ZEISS Auriga microscope equipped with an energy dispersive X-ray spectroscopy (EDX) detector or an ESEM FEI Quanta 200 microscope operating at 25 kV.

#### 2.2.6. Thermo-gravimetric analysis (TGA)

Thermo-gravimetric measurements were performed with Netzch 209 F1 Libra. The samples were heated from 25 °C to 800 °C (heating rate 10 °C/min) under constant nitrogen flux (20 mL/min).

#### 2.2.7. X-ray photoelectron spectroscopy (XPS)

XPS measurements were performed using a PHI 5000 Versaprobe instrument equipped with a monochromated Al K-alpha source (1486.6 eV). A double charge compensation system, comprised of an electron and $Ar^{\pm}$ ion gun, was used to neutralize surface charging. Survey and high resolution (HR) spectra were acquired using Pass Energy (PE) values of 187.85 and 23.50 eV, respectively. For these measurements (i) the C1s peak at 284.5 eV was chosen as the reference shift, (ii) a Shirley background function was subtracted from HR spectra to remove background signal, and (iii) pseudo-Voigt functions were used to deconvolute the HR curves.

#### 2.2.8. $N_2$ physisorption

$N_2$ physisorption characterization was performed using a Micrometrics ASAP 2020 Porosimeter at 77 K. Surface area and pore volume textural parameters were assessed by the Brunauer-Emmett-Teller and Barret-Joyner-Halenda methods, respectively [15].

#### 2.2.9. Cyclic voltammetric analysis

Cyclic voltammetries in KOH 0.1 M have been carried out in a three-electrode cell, in which $TiO_2$ or PhCN represented the working electrode, while a Pt-grid and a saturated calomel electrode (SCE, E = 0.268 V vs NHE) were used as counter and reference electrodes, respectively. The pH dependence of electrode potential was considered by the following relation E = E′ + 0.059 V * pH. A potentiostat-galvanostat (Metrohm Autolab 302 N Metrohm Switzerland), controlled by NOVA software was used to record the related data.

#### 2.2.10. X-ray diffraction

X-ray diffraction patterns were collected at room temperature by using a Rigaku Miniflex II diffractometer with θ-2θ Bragg-Brentano geometry with Cu Kα (λ = 1.5418 Å), radiation at room temperature.

### 2.3. Measurement of photocatalytic activity

The photocatalytic performance of the as-prepared samples was evaluated by monitoring the concentration changes in RhB aqueous solution under visible light irradiation. The photocatalytic performance was assessed using a white LED (white LED Philips 13 W with an optical power 100 mW) as the light source.

Before light irradiation, both the catalyst suspension (50 mg) and RhB (50 mL, 10 $mg{\cdot}L^{-1}$)/MB (50 mL, 10 $mg{\cdot}L^{-1}$) were stirred in the dark for 60 min to ensure absorption–desorption equilibrium between the catalyst and the dye. During the photodegradation process, 2 mL aliquots were collected every 120 min. The aliquots were then centrifuged and the residual concentrations of RhB and MB were analyzed using the UV–Vis-NIR Agilent Technologies Cary 5000 spectrophotometer.

## 3. Results and discussion

### 3.1. UV–Vis measurements

Fig. 1A shows the normalized UV–Vis absorption spectra for the three building blocks used to form the hybrid systems (i.e., $TiO_2$, g-$C_3N_4$, and PhCN). $TiO_2$ (i.e., anatase) strongly absorbs in the UV, showing a precipitous increase in the absorption for wavelengths shorter than 410 nm with band gap of 3.2 eV. With an absorption onset near 450 nm and a corresponding band gap of 2.7 eV, g-$C_3N_4$ exhibits an optical absorption that extends into the visible region. PhCN, due to the presence of phenyl groups within its structure, promotes a further redshift in the absorption edge, with a broad absorption band that begins at 600 nm and, hence, extends well into the visible region.

Fig. 1B shows the absorbance spectra for the two hybrid systems, where the PhCN/$TiO_2$ notably displays an absorption through the visible and UV regions while the g-$C_3N_4$/$TiO_2$ merely has an absorption onset near 450 nm. The different absorption behavior among the two composites evidence the increased working region between 400 and 600 nm. Another key difference between the two hybrid systems, which is highlighted in Fig. 1C, is that the spectrum for PhCN/$TiO_2$ appears as the sum of the two building blocks, featuring a large absorption band down to 600 nm, while the g-$C_3N_4$/$TiO_2$ hybrid does not. Instead, the g-$C_3N_4$/$TiO_2$ hybrid system tends to preserve the $TiO_2$ bandgap as a whole, showing only a red-shift in the absorption spectrum. This effect is related to the so-called “direct optical electron transfer” from the HOMO level of the organic part (g-$C_3N_4$) into the conduction band of $TiO_2$. In contrast, a “photoinduced electron transfer” is more likely for the PhCN/$TiO_2$ hybrid, where the absorption features are not expected to change with respect to the organic and inorganic building blocks [20]. Indeed, in this case the absorbed visible photon promotes the electron from the HOMO ground state into the LUMO excited state of the organic compound, followed by a fast electron transfer to the conduction band of $TiO_2$. With most Gratzel-type solar cells reliant on this mechanism, it is conceivable that the PhCN/$TiO_2$ system will be applicable to this field as well [25].

### 3.2. Morphological and compositional analysis

Fig. 2A and B shows SEM images of the PhCN/$TiO_2$ hybrid system that reveals spherically-shaped structures with micrometer-scale dimensions. Large aggregates are absent from the images. To further confirm the absence of undesirable clusters of $TiO_2$ and PhCN, EDAX analysis was performed. Nitrogen, rather than carbon, was used as the indicator for PhCN since carbon is present in the glue support. The EDAX analysis for the trace denoted in Fig. 2B yields the elemental profile shown in Fig. 2C. The data shows a precise overlap of the inorganic and organic components, where further scans showed no evidence of building block clusters or any sort of spread distribution of the organic component. N-adsorption BET analysis (Table 1, supporting S1), as expected, indicates that the hybrid structures have a lower specific surface and pore volume compared to pure $TiO_2$.

### 3.3. TGA analysis

To determine the PhCN content in the final product, thermogravimetric analysis was performed from room temperature to 800 °C (Supporting information, S2). The PhCN phase in the hybrid PhCN/$TiO_2$ sample becomes unstable when the heat temperature is around 500 °C. According to [24], the weight loss is associated to the loss of the phenyl groups in the heptazinic system of the PhCN. The weight loss in the range of 500–800 °C is about 1% and can be correlated to the percentage in weight of the PhCN in the hybrid system.

### 3.4. XPS analysis

Fig. 3 compares the XPS survey spectra taken for $TiO_2$ to the as prepared heterostructure composites where all of the detected elements are highlighted. The $TiO_2$ spectrum, as expected, exhibits sharp Ti and O elemental photoelectron peaks at binding energies of 458.2 (Ti2p) and 529.5 eV (O1s), respectively [26]. The carbon peak at 284.5 eV is attributed to the residual carbon from the sample preparation precursors and adventitious carbon from ambient exposure. The spectra for

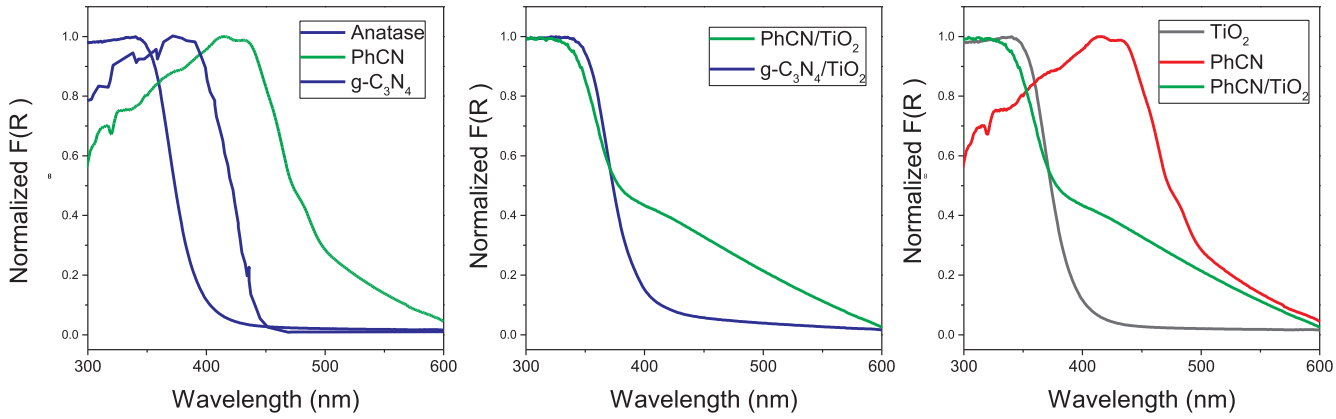


**Fig. 1.** Normalized absorption spectra of $TiO_2$ (anatase), g-$C_3N_4$, and PhCN (i.e., the building blocks for the hybrid systems) (A), the hybrid systems g-$C_3N_4$/$TiO_2$ and PhCN/$TiO_2$ (B), and the differential absorption of PhCN/$TiO_2$ from building blocks (C).

the two hybrid samples (i.e., $TiO_2$/PhCN and $TiO_2$/g$C_3N_4$) reveal the presence of a N1s peak (also see Fig. 4D for an enlarged spectrum), where the relative percentages observed (0.7 at.% for $TiO_2$/PhCN and 1.2 at.% for $TiO_2$/g$C_3N_4$) are consistent with the quantity of nitrogen included in the two preparations.

Fig. 4 shows high resolution (HR) XPS spectra for major peaks observed in the various measurements. The Ti2p spectrum (Fig. 4A) for the $TiO_2$ sample confirms that $TiO_2$ is present in the anatase phase [27]. The two composites show Ti2p peaks, which apart from a slight shift toward higher binding energies ($\Delta$ = 0.3 eV), overlap with the bare $TiO_2$ peaks. The observed shift is due to a surface charging phenomenon related to the reduction of an anionic surface layer [28]. The same shift to higher binding energies is also clearly visible in the O1s spectrum (Fig. 4C and D). This same spectrum also reveals a 531.0 eV component that is related to OH species adsorbed onto the $TiO_2$ surface (Fig. 4B, inset). This component is, as expected, lessoned for the two composite samples (20% for $TiO_2$ compared to 15% for the composites) due to a loss in $TiO_2$ surface area. The C1s spectrum in both hybrid systems (Fig. 4B) exhibits four major peaks centred at 284.5, 286.0, 288.5, and

**Table 1**
BET analysis of pure $TiO_2$ and PhCN/$TiO_2$ hybrid system.

| Sample | $S_{BET}$ ($m^2 \cdot g^{-1}$) | $V_{PORES}$ ($cm^3 \cdot g^{-1}$) |
|---|---|---|
| $TiO_2$ | 244 | 0.35 |
| PhCN/$TiO_2$ | 126 | 0.17 |
| g-$C_3N_4$/$TiO_2$ | 219 | 0.30 |

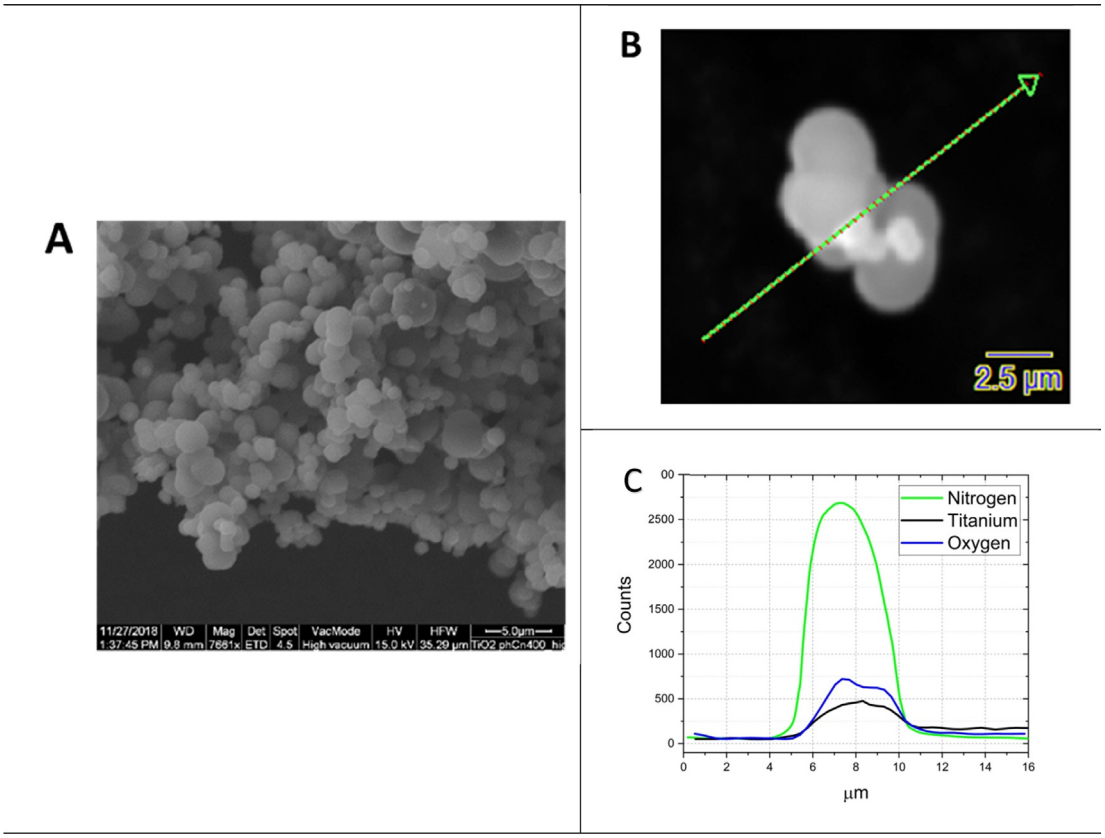


**Fig. 2.** SEM images of PhCN/$TiO_2$ hybrid system taken at low (A) and high magnification (B) and EDX analysis for the cross section denoted by the dashed green arrow (C).

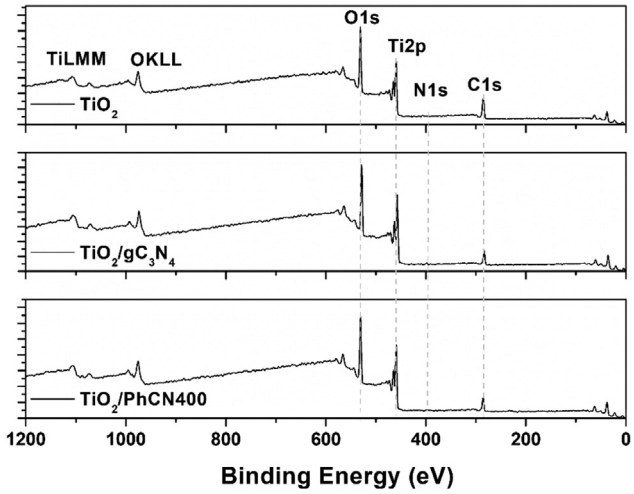


**Fig. 3.** XPS survey spectra for the bare $TiO_2$, $TiO_2/gC_3N_4$, and $TiO_2$/PhCN400.

289.4 eV that correspond to C—C, C-N (and possibly to C—O—C or C—OH bonds), carbon in pyridinic bonds with nitrogen, and O═C—O carboxylic bonds, respectively [29]. The N1s spectrum (Fig. 4E and F) reveals the characteristic $sp^2$ hybridized N peaks reported and ascribed to pyridinic nitrogen (398.6 eV) and N-$(C)_3$ amino groups (400.0 eV) [29]. Taken together, the XPS analysis confirms the presence of $TiO_2$, g-$C_3N_4$, and PhCN in the composite materials. The results, therefore, provide further evidence that heterostructures have been successfully formed, in agreement with the results obtained by UV–VIS reflectance measurements and TRPL (vide infra).

### 3.5. Structural characterization

The Raman spectrum of PhCN (Supporting information, S3) reports the most characteristic figures between 1350 and 1650 $cm^{-1}$. The most intense bands, at 1601 $cm^{-1}$ and 1392 $cm^{-1}$ have been assigned to the motion of the phenyl group and to conjugated stretching vibration (C—C) between the phenyl ring and the triazine ring, respectively [24]. This part of the spectrum is not overlapped with the very intense contribution of Anatase that shows four main Raman peaks at 144, 397, 516 and 639 $cm^{-1}$, assigned to the Eg, B1g, A1g and Eg vibrational modes of the anatase crystal phase (Supporting information, S4). The hybrid materials still show the Raman figures of the polymer without significant shift [30] (Supporting information, S5).

The XRD spectrum of TiO2 reports the diffraction peak of Anatase [30]. No secondary phases have been observed (Supporting information, S6). According to [24] The XRD pattern of PhCN sample report a well-defined peak at about 27.6° assigned to (001) reflection and a broad peak at about 13°, related to the reflection from (210) plane (Supporting information, S7). The diffraction pattern of the hybrid sample has been recorded as well, however, the low content of polymer (estimated in 1% from TGA analysis) was not enough to be observed (Supporting information, S8).

### 3.6. Photoluminescence measurements

Fig. 5 shows the comparison of the photoluminescence spectra of PhCN to the PhCN/$TiO_2$ hybrid system for a static excitation at 405 nm, where the observed emission is arbitrarily normalized to allow an easier comparisons of the spectral line shape. The overall emission of the PHCN is about two order of magnitude higher with respect the PL intensity of the PHCN/$TiO_2$ sample. Upon band-to-band excitation, the radiative channel in PhCN is mainly due to recombination from (i) σ* to LP, (ii) π* to LP, and (iii) π* to π levels, generating a broad emission peaked at about 530 nm. The radiative recombination path presents an optical quantum yield of approximately 60% that, considering the spectral range involved, makes the PhCN a highly promising candidate material for lighting applications [24]. In contrast, the PhCN/$TiO_2$ hybrid system displays a weak emission, which when prepared under comparable experimental conditions, is less than 1% of that of the pure compound. The hybrid also displays a red shift compared to the PhCN sample. It should be noted that the applied excitation energy is below the band gap of anatase, and as such, the contribution from the inorganic component is excluded. The defect-related luminescence band in $TiO_2$ is, in fact, centered near 470 nm and, thus, the recorded luminescence in the PhCN/$TiO_2$ hybrid is largely related to the organic component [31].

Time-resolved photoluminescence measurements were carried out on PhCN and the PhCN/$TiO_2$ hybrid

It is now important to gather more information about these results by specific measurement on the kinetics of the radiative decay paths, so that to further understand the interaction between PhCN and $TiO_2$ time resolved measurements were performed.

Fig. 6 shows a comparison of the two decay profiles obtained using a 410 nm excitation wavelength acquired over a 100 ns time window. Previously, we showed that the decay time of pure PhCN evidences the presence of at least two contributions, one peaked at high energy and characterized by a relatively fast decay (30–40 ns), and the other, a low energy contribution with a considerably slower decay time (200–250 ns). These two bands are related to the σ* and π* excited levels, respectively [19,24]. It is interesting to note that, from a phenomenological point of view, the same trend is observed for g-$C_3N_4$ where there are still two main components emitting in two separate spectral regions [17]. The main difference, however, is that the recombination kinetics for g-$C_3N_4$ are significantly faster for both excitations, being less than 1 and 5 ns, respectively [17]. The higher recombination rate of photogenerated electron–hole pairs in g-$C_3N_4$ is one of the main bottlenecks in the use of g-$C_3N_4$ as a photocatalyst [32–34]. From this perspective, the slower trend of PhCN is a characteristic that is expected to enhance the photocatalytic activity of the PhCN/$TiO_2$ hybrid as compared to the g-$C_3N_4$/$TiO_2$ hybrid.

Fig. 6 also shows that the PhCN/$TiO_2$ hybrid displays a much faster decay profile compared to PhCN. The decay time profiles can be well-represented by a multiexponential decay function:

$$y = y_0 + \sum_i A_i e^{-\frac{t}{\tau_i}}$$

with

$$\frac{1}{\tau_i} = \frac{1}{\tau_{Ri}} + \frac{1}{\tau_{NRi}} = \gamma_{Ri} + \gamma_{NRi}$$

where $i = 1$ or 2, $\tau_r$ and $\tau_{nr}$ represent radiative and non-radiative lifetime contribution to the overall decay time $\tau$, and $\gamma_R$ and $\gamma_{NR}$ are the probabilities for radiative and non-radiative recombination. Fit results and decay parameters for PhCN and PhCN/$TiO_2$ are reported in Table 2. The smaller overall time decay for the PhCN/$TiO_2$ hybrid is a direct consequence of an increase in the non-radiative component, which is often correlated with a decrease in the luminescence intensity, as is observed for the present case (Fig. 5). These results, which agree with the above reported absorption measurements, strongly suggest the formation of an efficient fast transfer from the LUMO state of the polymeric PhCN structure to the conduction band of $TiO_2$. Both the excited levels σ* and π* are involved in the non-radiative process, realizing a faster decay time constant and suggesting a process that involves electrons transfer from the organic component, which acts as a sensitizer, to the $TiO_2$ component, which acts as an activator. This energy transfer process affects, in a direct way, the photocatalytic properties (vide infra).

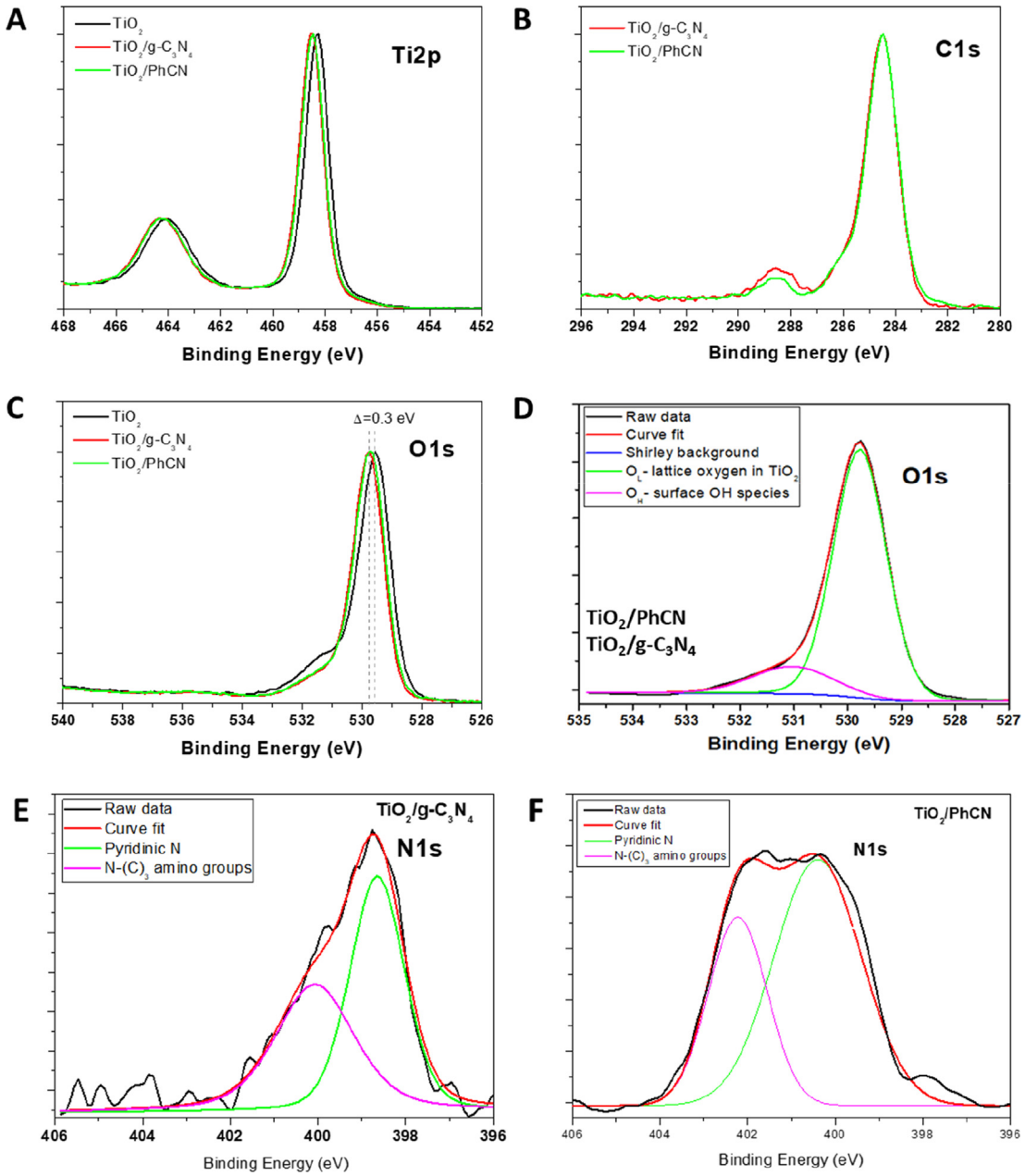


**Fig. 4.** HR XPS showing the Ti2p (A), C1s (B), O1s (C,D), and N1s (E,F) photoelectronic peaks. (D) shows the result of a deconvolution procedure that was applied to all the samples. The procedure is similarly applied to the N1s $TiO_2$ + $gC_3N_4$ data shown in (D) and N1s $TiO_2$ + $gC_3N_4$ data shown in (F).

## 4. Photocatalytic performance

$TiO_2$, g-$C_3N_4$/$TiO_2$, and PhCN/$TiO_2$ were assessed as photocatalysts for the photodegradation of RhB and MB under white LED irradiation.

Most of the emitted light from this source has an energy below 2.8 eV, and, therefore, cannot be absorbed by the anatase phase of $TiO_2$ (band gap = 3.0 eV). It can, however, be efficiently absorbed by PhCN, while only a limited amount of absorption occurs for g-$C_3N_4$ (band gap = 2.7 eV).

Fig. 7A shows the normalized RhB concentration as a function of time for the three photocatalysts studied. As anticipated, both $TiO_2$ and the g-$C_3N_4$/$TiO_2$ hybrid show poor photocatalytic activity toward the photodegradation of RhB. In stark contrast, the PhCN/$TiO_2$ hybrid system is remarkably effective, a capability that is attributed to the broad absorption that PhCN displays in the visible range and to the efficiency by which the PhCN/$TiO_2$ system separates charge upon light excitation.

We calculated the yield of the photoreaction obtained after 12 h of continuous irradiation with a white LED in solution 10 mg/L of Rhodamine B.

The degradation efficiency was about 4% by using pure $TiO_2$ as catalyst, 3% only PHCN. The degradation efficiency of PHCN in dark condition remain below 4%. The efficiency increases to 17% by using only g-$C_3N_4$/$TiO_2$. When the hybrid PHCN/TiO2 catalyst is exploited as catalyst under continuous illumination the degradation efficiency increases to 98% and 88% for Rhodamine B and methylene Blue, respectively (4% in dark conditions).

The photoconversion efficiency calculated at 420 nm for MB, defined as the ratio between number of degraded molecules and the number of adsorbed photons was about 20%, relatively high, considering for monochromatic visible light (Supporting information, S9).

Furthermore, the kinetics characteristic of RhB degradation under visible light irradiation over all the as-prepared samples was investigated by using the simplified Langmuir-Hinshelwood model ln(C/

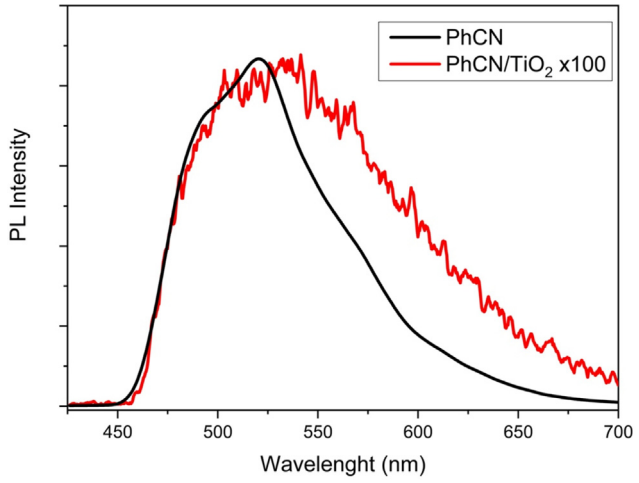


**Fig. 5.** Normalized photoluminescence measurements of PhCN and the PhCN/$TiO_2$ hybrid system. The intensity of the PhCN/$TiO_2$ is about 100 time less with respect the pure PhCN.

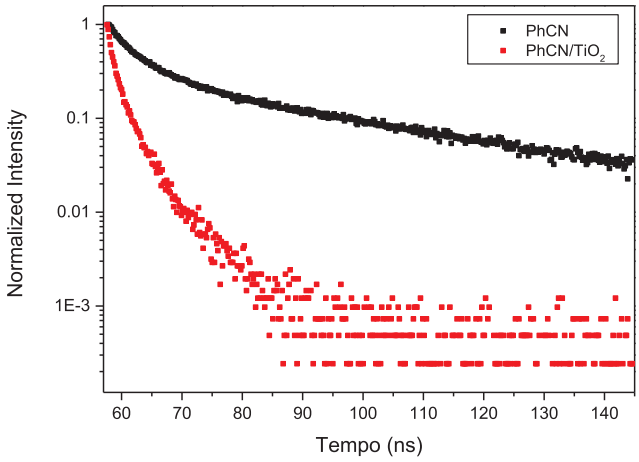


**Fig. 6.** Time-resolved photoluminescence showing decay profiles for PhCN and the PhCN/$TiO_2$ hybrid system.

**Table 2**
Decay parameters for PhCN and PhCN/$TiO_2$.

| Sample | $t_1$ (ns) | $t_2$ (ns) |
|---|---|---|
| PhCN | 40 | 250 |
| PhCN/$TiO_2$ | 1.4 | 4.6 |

$C_0$) = kt, where k is the first-order rate constant ($min^{-1}$), $C_0$ represents the initial concentration of RhB solution and C represents the concentration of RhB solution during photocatalytic process. As shown in Fig. 7B the kinetic constant of PhCN/$TiO_2$ sample is much higher than that of the other samples. The calculated kinetic constants are $4.41 \times 10^{-3}$ $min^{-1}$, $2.94 \times 10^{-4}$ $min^{-1}$ and $5.50 \times 10^{-5}$ $min^{-1}$ for PhCN/$TiO_2$, g-$C_3N_4$/$TiO_2$ and $TiO_2$ respectively.

The photoconversion efficiency calculated at 420 nm for MB, defined as the ratio between number of degraded molecules and the number of adsorbed photons was about 20%, relatively high, considering for monochromatic visible light (Supporting information, S9).

The stability of the PhCN/$TiO_2$ composite was evaluated for the MB photodegradation. The removal rate of MB was 87.2, 80, 76.5 and 76% respectively when the catalyst is subjected to 4-cycle consecutive photocatalytic tests. After each photocatalytic test the catalyst was washed several times with distilled water and dried before running the consecutive test.

As it was already state, the increased photocatalytic activity of the hybrid composites is due to higher charge separation in the photocatalysts. The behaviour of the structure can be described taking into account the related position of CB and VB of the two components. In this regard, information on the location of the conduction band edge can be derived by the reduction potential measured by the cyclic-voltammetry method [35]. Actually, due to the fact that during the oxidation or reduction process charges are injected/taken to/from the material, reconfiguration of the structure may appear. Thus, the onset values of the oxidation as well as reduction wave are considered as the band gap edges [36]. In the present case, reductive currents were observed at values of −0.85 V vs SCE (saturated calomel electrode) at $TiO_2$ in alkaline solution, which is in agreement with analogous data derived in previous work for $TiO_2$ samples either as nano-powders [37] or nanotubular structures [38,39]. The value of −1.11 V was instead measured when PhCN was used as cathodic material. On these bases, values of −0.43 V and −0.268 V (vs (Normal Hydrogen Electrode, NHE, in neutral solution) have been evaluated as the LUMO for PhCN and CB edge of $TiO_2$, respectively (Supporting information, S10).

Fig. 8 shows a schematic representation of the photoexcited electrons transfer process from the LUMO state of PhCN to the conduction band of $TiO_2$. Here, it is assumed that PhCN, like g-$C_3N_4$, is an intrinsic semiconductor with the Fermi level positioned in the middle of the bandgap at +0.25 V vs. NHE [34]. Then, taking its band gap to be 2.0 eV, the LUMO state is positioned at −0.43 eV vs NHE, a value that is almost resonant with the $TiO_2$ conduction band (-0.27 eV vs NHE). In such a scenario, the HOMO level for PhCN is located at 1.57 eV vs NHE while the corresponding valence band of $TiO_2$ is at 2.93 eV vs NHE [40]. Because of the relative position of the LUMO state with respect to the conduction band of $TiO_2$, the charge transfer from the organic component to $TiO_2$ is facilitated, while the holes remain in the HOMO state of PhCN, further increasing the charge separation of the

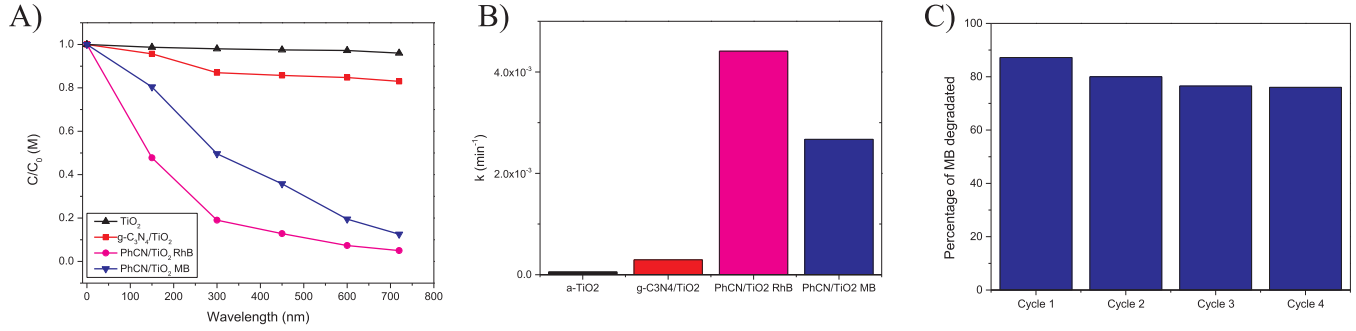


**Fig. 7.** Time dependence of the normalized RhB and MB concentration under white LED irradiation when using $TiO_2$ (anatase), g-$C_3N_4$/$TiO_2$, and PhCN/$TiO_2$ as photocatalysts (A) and reaction rate constant (k) by employing $TiO_2$ (anatase), g-$C_3N_4$/$TiO_2$, and PhCN/$TiO_2$ as photocatalysts respectively (B). The stability of the catalyst is reported for the MB photodegradation (C).

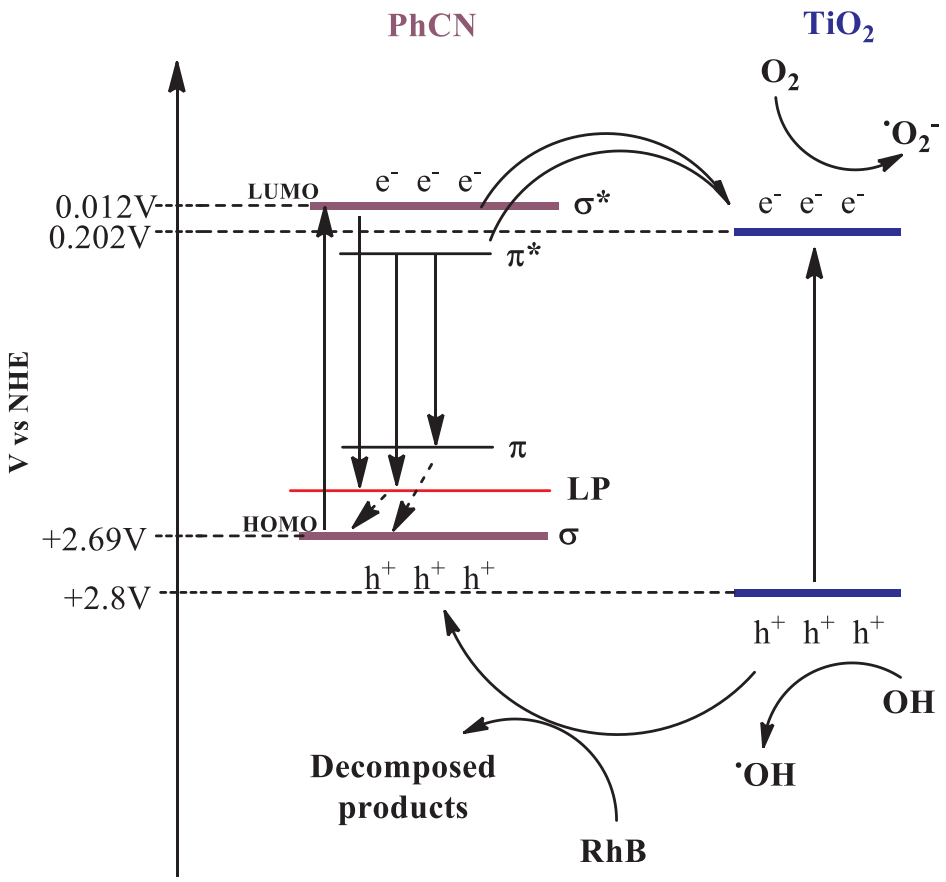


**Fig. 8.** Scheme showing the process by which photoexcited electrons are transferred from the LUMO state of PhCN to the conduction band of $TiO_2$.

photogenerated electron-hole pairs. The electrons of the excited states can then react with oxygen to create superoxide and hydroxyl radicals. The low band gap of PhCN, and its associated absorption over much of the visible spectrum, therefore, gives rise to a heterostructure with $TiO_2$ that makes the PhCN/$TiO_2$ hybrid composite a very promising photocatalyst, not only for RhB photodegradation, but also for the neutralization of air pollutants. Such a photocatalyst could be activated by the solar radiation, or alternatively, where the UV component must be filtered out such as in LED-based indoor lighting applications.

## 5. Conclusions

In conclusion, we have prepared a new PhCN/$TiO_2$ hybrid system using a hydrothermal synthesis followed by calcination. XPS, SEM, and EDX analysis all reveal that the heterostructure has been successfully formed. Optical absorption as well as steady state and time-resolved photoluminescence show an optical response that is in accordance with photocatalytic activity where synergies exist between both material segments of the hybrid structure. A high level of photocatalytic activity was demonstrated using a well-established model reaction illuminated only with visible light. The work, therefore, advances the PhCN/$TiO_2$ hybrid as a promising new system for catalysing green chemistry powered by the sun.

## CRediT authorship contribution statement

**Stefania Porcu:** Conceptualization, Methodology, Investigation, Writing - original draft. **Micaela Castellino:** Investigation. **Ignazio Roppolo:** Investigation. **Carlo Maria Carbonaro:** Investigation, Writing - review & editing. **Simonetta Palmas:** Investigation. **Laura Mais:** Investigation. **Maria Francesca Casula:** Investigation. **Svetlana Neretina:** Writing - review & editing, Funding acquisition. **Robert A. Hughes:** Writing - review & editing. **Francesco Secci:** Investigation, Writing - review & editing. **Pier Carlo Ricci:** Conceptualization, Methodology, Investigation, Supervision, Writing - review & editing, Supervision, Project administration, Funding acquisition.

## Declaration of Competing Interest

The authors declare that they have no known competing financial interests or personal relationships that could have appeared to influence the work reported in this paper.

## Acknowledgements

This work is supported by the “Fondazione di Sardegna” within the project L.R 7. CUP F74I19000930007 “NG-Light: a new generation of phosphors”. The authors acknowledge the CeSAR (Centro Servizi d’Ateneo per la Ricerca) of the University of Cagliari, Italy for the Time Resolved Photoluminescence experiments. The work carried out at Notre Dame is supported by a National Science Foundation Award (DMR-1803917) to S.N.

## Appendix A. Supplementary material

Supplementary data to this article can be found online at https://doi.org/10.1016/j.apsusc.2020.147394.

## References

[1] M. Huang, J. Yu, Q. Hu, W. Su, M. Fan, B. Li, L. Dong, Preparation and enhanced photocatalytic activity of carbon nitride/titania(001 vs 101 facets)/reduced graphene oxide (g-$C_3N_4$/$TiO_2$/rGO) hybrids under visible light, Appl. Surf. Sci. 389 (2016) 1084–1093, https://doi.org/10.1016/j.apsusc.2016.07.180.

[2] T.A. Gadhi, S. Hernández, M. Castellino, P. Jagdale, T. Husak, A. Hernández-Gordillo, A. Tagliaferro, N. Russo, Insights on the role of β-$Bi_2O_3$/$Bi_5O_7NO_3$ heterostructures synthesized by a scalable solid-state method for the sunlight-driven photocatalytic degradation of dyes, Catal. Today. 321–322 (2019) 135–145, https://doi.org/10.1016/j.cattod.2017.12.038.

[3] Y. Li, K. Lv, W. Ho, F. Dong, X. Wu, Y. Xia, Hybridization of rutile $TiO_2$ ($rTiO_2$) with g-$C_3N_4$ quantum dots (CN QDs): an efficient visible-light-driven Z-scheme hybridized photocatalyst, Appl. Catal. B Environ. 202 (2017) 611–619, https://doi.org/10.1016/j.apcatb.2016.09.055.

[4] K. Nakata, A. Fujishima, TiO 2 photocatalysis: design and applications, J. Photochem. Photobiol. C Photochem. Rev. 13 (2012) 169–189, https://doi.org/10.1016/j.jphotochemrev.2012.06.001.

[5] R. Solarska, A. Królikowska, J. Augustyński, Silver nanoparticle induced photocurrent enhancement at WO3 photoanodes, Angew. Chem. Int. Ed. 49 (2010) 7980–7983, https://doi.org/10.1002/anie.201002173.

[6] S. Palmas, P.A. Castresana, L. Mais, A. Vacca, M. Mascia, P.C. Ricci, $TiO_2$-$WO_3$ nanostructured systems for photoelectrochemical applications, RSC Adv. 6 (2016) 101671–101682, https://doi.org/10.1039/c6ra18649a.

[7] A. Kay, I. Cesar, M. Grätzel, New benchmark for water photooxidation by nanostructured α-$Fe_2O_3$ films, J. Am. Chem. Soc. 128 (2006) 15714–15721, https://doi.org/10.1021/ja064380l.

[8] M.R. Hoffmann, S.T. Martin, W. Choi, D.W. Bahnemann, Environmental applications of semiconductor photocatalysis, Chem. Rev. 95 (1995) 69–96, https://doi.org/10.1021/cr00033a004.

[9] Y. Nosaka, S. Komori, K. Yawata, T. Hirakawa, A.Y. Nosaka, Photocatalytic •OH radical formation in $TiO_2$ aqueous suspension studied by several detection methods, Phys. Chem. Chem. Phys. 5 (2003) 4731–4735, https://doi.org/10.1039/b307433a.

[10] A. Jańczyk, E. Krakowska, G. Stochel, W. Macyk, Singlet oxygen photogeneration at surface modified titanium dioxide, J. Am. Chem. Soc. 128 (2006) 15574–15575, https://doi.org/10.1021/ja065970m.

[11] S. Yadav, G. Jaiswar, Review on undoped/doped $TiO_2$ nanomaterial; synthesis and photocatalytic and antimicrobial activity, J. Chinese Chem. Soc. 64 (2017) 103–116, https://doi.org/10.1002/jccs.201600735.

[12] S.A. Ansari, M.M. Khan, M.O. Ansari, M.H. Cho, Nitrogen-doped titanium dioxide (N-doped $TiO_2$) for visible light photocatalysis, New J. Chem. 40 (2016) 3000–3009, https://doi.org/10.1039/c5nj03478g.

[13] L.K. Preethi, R.P. Antony, T. Mathews, L. Walczak, C.S. Gopinath, A study on doped heterojunctions in $TiO_2$ nanotubes: an efficient photocatalyst for solar water splitting, Sci. Rep. 7 (2017), https://doi.org/10.1038/s41598-017-14463-0.

[14] S. Palmas, A.M. Polcaro, J.R. Ruiz, A. Da Pozzo, A. Vacca, M. Mascia, F. Delogu, P.C. Ricci, Effect of the mechanical activation on the photoelectrochemical properties of anatase powders, Int. J. Hydrogen Energy 34 (2009) 9662–9670, https://doi.org/10.1016/j.ijhydene.2009.07.058.

[15] S.G. Kumar, K.S.R.K. Rao, Comparison of modification strategies towards enhanced charge carrier separation and photocatalytic degradation activity of metal oxide semiconductors ($TiO_2$, $WO_3$ and ZnO), Appl. Surf. Sci. 391 (2017) 124–148, https://doi.org/10.1016/j.apsusc.2016.07.081.

[16] S.C. Yan, Z.S. Li, Z.G. Zou, Photodegradation performance of g-$C_3N_4$ fabricated by directly heating melamine, Langmuir 25 (2009) 11269–11273, https://doi.org/10.1021/la900923z.

[17] L. Stagi, D. Chiriu, C.M. Carbonaro, R. Corpino, P.C. Ricci, Structural and optical properties of carbon nitride polymorphs, Diam. Relat. Mater. 68 (2016) 84–92, https://doi.org/10.1016/j.diamond.2016.06.009.

[18] L. Stagi, D. Chiriu, C.M. Carbonaro, R. Corpino, P.C. Ricci, Structural and optical properties of carbon nitride polymorphs, Diam. Relat. Mater. 68 (2016) 84–92, https://doi.org/10.1016/j.diamond.2016.06.009.

[19] Y. Zhang, Q. Pan, G. Chai, M. Liang, G. Dong, Q. Zhang, J. Qiu, Synthesis and luminescence mechanism of multicolor-emitting g-C3N4 nanopowders by low temperature thermal condensation of melamine, Sci. Rep. 3 (2013) 1943, https://doi.org/10.1038/srep01943.

[20] M. Bledowski, L. Wang, A. Ramakrishnan, O.V. Khavryuchenko, V.D. Khavryuchenko, P.C. Ricci, J. Strunk, T. Cremer, C. Kolbeck, R. Beranek, Visible-light photocurrent response of TiO2–polyheptazine hybrids: evidence for interfacial charge-transfer absorption, Phys. Chem. Chem. Phys. 13 (2011) 21511, https://doi.org/10.1039/c1cp22861g.

[21] J. Wen, J. Xie, X. Chen, X. Li, A review on g-$C_3N_4$ -based photocatalysts, Appl. Surf. Sci. 391 (2017) 72–123, https://doi.org/10.1016/j.apsusc.2016.07.030.

[22] X. Yang, F. Qian, G. Zou, M. Li, J. Lu, Y. Li, M. Bao, Facile fabrication of acidified g-$C_3N_4$/g-$C_3N_4$ hybrids with enhanced photocatalysis performance under visible light irradiation, Appl. Catal. B Environ. 193 (2016) 22–35, https://doi.org/10.1016/j.apcatb.2016.03.060.

[23] L. Zhou, L. Wang, J. Zhang, J. Lei, Y. Liu, The preparation, and applications of g-$C_3N_4$/$TiO_2$ heterojunction catalysts—a review, Res. Chem. Intermed. 43 (2017) 2081–2101, https://doi.org/10.1007/s11164-016-2748-8.

[24] S. Porcu, I. Roppolo, M. Salaun, G. Sarais, S. Barbarossa, M.F. Casula, C.M. Carbonaro, P.C. Ricci, Come to light: detailed analysis of thermally treated phenyl modified carbon nitride polymorphs for bright phosphors in lighting applications, Appl. Surf. Sci. 504 (2020) 144330, , https://doi.org/10.1016/j.apsusc.2019.144330.

[25] D.F. Watson, G.J. Meyer, Electron injection at dye-sensitized semiconductor electrodes, Annu. Rev. Phys. Chem. 56 (2005) 119–156, https://doi.org/10.1146/annurev.physchem.56.092503.141142.

[26] C. Ocal, S. Ferrer, Low temperature diffusion of Pt and Au atoms through thin $TiO_2$ films on a Ti substrate, Surf. Sci. 191 (1987) 147–156, https://doi.org/10.1016/S0039-6028(87)81053-1.

[27] C. Badini, S.M. Deambrosis, O. Ostrovskaya, V. Zin, E. Padovano, E. Miorin, M. Castellino, S. Biamino, Cyclic oxidation in burner rig of TiAlN coating deposited on Ti-48Al-2Cr-2Nb by reactive HiPIMS, Ceram. Int. 43 (2017) 5417–5426, https://doi.org/10.1016/j.ceramint.2017.01.031.

[28] A. Naldoni, M. Allieta, S. Santangelo, M. Marelli, F. Fabbri, S. Cappelli, C.L. Bianchi, R. Psaro, V. Dal Santo, Effect of nature and location of defects on bandgap narrowing in black $TiO_2$ nanoparticles, J. Am. Chem. Soc. 134 (2012) 7600–7603, https://doi.org/10.1021/ja3012676.

[29] P.C. Ricci, N. Laidani, D. Chiriu, M. Salis, C.M. Carbonaro, R. Corpino, ALD growth of metal oxide on carbon nitride polymorphs, Appl. Surf. Sci. 456 (2018) 83–94, https://doi.org/10.1016/j.apsusc.2018.06.021.

[30] P.C. Ricci, C.M. Carbonaro, A.G. Lehmann, F. Congiu, B. Puxeddu, G. Cappelletti, F. Spadavecchia, Structure and photoluminescence of $TiO_2$ nanocrystals doped and co-doped with N and rare earths (y3+, pr3+), J. Alloys Compd. 561 (2013) 109–113, https://doi.org/10.1016/j.jallcom.2013.01.164.

[31] L. Stagi, C.M. Carbonaro, R. Corpino, D. Chiriu, P.C. Ricci, Light induced $TiO_2$ phase transformation: Correlation with luminescent surface defects, Phys. Status Solidi 252 (2015) 124–129, https://doi.org/10.1002/pssb.201400080.

[32] J. Wen, J. Xie, X. Chen, X. Li, A review on g-$C_3N_4$-based photocatalysts, Appl. Surf. Sci. 391 (2017) 72–123, https://doi.org/10.1016/j.apsusc.2016.07.030.

[33] M. Ismael, Y. Wu, A mini-review on the synthesis and structural modification of g-$C_3N_4$-based materials, and their applications in solar energy conversion and environmental remediation, Sustain. Energy Fuels 3 (2019) 2907–2925, https://doi.org/10.1039/c9se00422j.

[34] S. Patnaik, S. Martha, S. Acharya, K.M. Parida, An overview of the modification of g-$C_3N_4$ with high carbon containing materials for photocatalytic applications, Inorg. Chem. Front. 3 (2016) 336–347, https://doi.org/10.1039/c5qi00255a.

[35] H. Liu, J. Tang, I.J. Kramer, R. Debnath, G.I. Koleilat, X. Wang, A. Fisher, R. Li, L. Brzozowski, L. Levina, E.H. Sargent, Electron acceptor materials engineering in colloidal quantum dot solar cells, Adv. Mater. 23 (2011) 3832–3837, https://doi.org/10.1002/adma.201101783.

[36] E. Kuçur, W. Bücking, T. Nann, Electrochemical determination of mesoscopic phenomena, defect states in CdSe nanocrystals and charge carrier manipulability, Microchim. Acta 160 (2008) 299–308, https://doi.org/10.1007/s00604-007-0899-4.

[37] E. Arca, G. Mulas, F. Delogu, J. Rodriguez-Ruiz, S. Palmas, The influence of mechanical processing on the photoelectrochemical behaviour of $TiO_2$ powders, J. Alloys Compd. 477 (2009) 583–587, https://doi.org/10.1016/j.jallcom.2008.10.120.

[38] R. Matarrese, M. Mascia, A. Vacca, L. Mais, E. Usai, M. Ghidelli, L. Mascaretti, B. Bricchi, V. Russo, C. Casari, A. Li Bassi, I. Nova, S. Palmas, Integrated Au/$TiO_2$ nanostructured photoanodes for photoelectrochemical organics degradation, Catalysts 9 (2019) 340, https://doi.org/10.3390/catal9040340.

[39] S. Palmas, A. Da Pozzo, M. Mascia, A. Vacca, P.C. Ricci, R. Matarrese, On the redox behaviour of glycerol at $TiO_2$ electrodes, J. Solid State Electrochem. 16 (2012) 2493–2502, https://doi.org/10.1007/s10008-012-1667-x.

[40] L. Kavan, M. Grätzel, S.E. Gilbert, C. Klemenz, H.J. Scheel, Electrochemical and photoelectrochemical investigation of single-crystal anatase, J. Am. Chem. Soc. 118 (1996) 6716–6723, https://doi.org/10.1021/ja954172l.